

Star formation in high redshift galaxies including Supernova feedback: effect on stellar mass and luminosity functions

Saumyadip Samui*

Department of Physics, Presidency University, 86/1 College Street, Kolkata - 700073, India.

Abstract

We present a semi-analytical model of high redshift galaxy formation. In our model the star formation inside a galaxy is regulated by the feedback from supernova (SNe) driven outflows. We derive a closed analytical form for star formation rate in a single galaxy taking account of the SNe feedback in a self-consistent manner. We show that our model can explain the observed correlation between the stellar mass and the circular velocity of galaxies from dwarf galaxies to massive galaxies of $10^{12} M_{\odot}$. For small mass dwarf galaxies additional feedback other than supernova feedback is needed to explain the spread in the observational data. Our models reproduce the observed 3-D fundamental correlation between the stellar mass, gas phase metallicity and star formation rate in galaxies establishing that the SNe feedback plays a major role in building this relation. Further, the observed UV luminosity functions of Lyman-Break galaxies (LBGs) are well explained by our feedback induced star formation model for a vast redshift range of $1.5 \leq z \leq 8$. In particular, the flattening of the luminosity functions at the low luminosity end naturally arises due to our explicit SNe feedback treatment.

Key words: galaxies: high-redshift; galaxies: star formation; stars: winds, outflows; galaxies: luminosity function;

1. Introduction

Presently we possess a wealth of observations regarding the high redshift universe, thanks to present day technology. The galaxies are regularly being detected till redshift $z \sim 10$ using Lyman Break technique (Steidel et al., 2003). The UV luminosity functions of Lyman break galaxy (LBG) are well constrained upto redshift $z \sim 8$ using Hubble Ultra deep field observations (Bouwens et al., 2007; Bouwens et al. 2008; Reddy & Steidel, 2009; Oesch et al., 2010; Bouwens et al., 2011). The faint end slope of the UV luminosity functions is well established for $z \lesssim 6$ and it shows flattening of the luminosity function at low luminosity end. The presence of Gunn-Peterson (Gunn & Peterson, 1965) absorption in the spectrum of high redshift quasars tells us a transition from highly ionised inter galactic medium (IGM) to partially ionised IGM around redshift $z \sim 6$ (Wyithe, Loeb & Carilli, 2005; Fan et al., 2006; Mortlock et al., 2011). Also the electron scattering optical depth (τ_e) measured in the Cosmic Microwave Background Radiation (CMBR) by Wilkinson Microwave Anisotropy Probe (WMAP) constrains the reionization redshift to be $z_{re} = 10.4 \pm 1.2$ (Komatsu et al. 2011) for a step reionization scenario.

Further, the high resolution absorption spectra of quasars show the presence of metals in very low density IGM far away from galaxies. Metals are produced

*Department of Physics, Presidency University, 86/1 College Street, Kolkata - 700073, India.

Email address: ssamui@gmail.com (Saumyadip Samui)

inside galaxies and believed to be transported by outflows produced by the Supernova (SNe) explosions in the galaxy. The outflows are routinely being observed in low redshift galaxies as well as in high redshift galaxies (Martin, 1999; Pettini et al., 2001; Martin, 2005). These outflows are likely to expel metals along with a large amount of inter stellar medium (ISM). This, in turn, reduces the star formation in galaxies by reducing the available gas to form new generation of stars. Thus the supernovae give a negative feedback to the star formation by throwing out gas from galaxies in the form of galactic winds.

Not only that, outflows also regulate the amount of metals in galaxies. Starting from very early days, a tight correlation has been observed between luminosity and metallicity of galaxies (Lequeux et al. 1979). Later, a more fundamental correlation has been found between the stellar mass and gas phase metallicity of galaxies in the local universe (Garnett, 2002; Tremonti et al., 2004; Lee et al., 2006; Kewley & Ellison, 2008) as well as in high redshift galaxies (Savaglio et al., 2005; Erb et al., 2006; Mannucci et al., 2009; Mannucci et al., 2010). It has been observed that galaxies with higher stellar mass trend to have more metals compared to their lower stellar mass counterparts. Further observations of local as well as high redshift universe show that the luminosity-metallicity or mass metallicity relation observed in galaxies is due to a more general relationship between stellar mass, metallicity of the gas and star formation rate (Mannucci et al. 2010; Cullen et al. 2013). Since, the outflows from galaxies throw metal enrich gas it is most likely that outflows play an important role in building up this correlation (Kobayashi et al., 2007; Scannapieco et al., 2008).

It has been seen from observations that the amount of gas/ISM expelled from a galaxy due to outflows is inversely proportional to the mass of the galaxy (Martin, 1999; Martin 2005). This is expected if the hot gas produced in SNe explosions drives the outflow. Roughly 10% of total SNe energy would be available for driving the outflow when the SNe remnants started to overlap with each other (Cox, 1972). The conservation of SNe energy available to drive the outflow to the kinetic energy of outflowing gas would lead to a mass outflow rate inversely proportional to the square of the circular velocity (v_c) of the galaxy. Even if the hot gas loses its thermal energy due to radiative cooling the momentum of the gas and/or the cosmic rays produced in the SNe shocks can still drive the outflow (Samui et al., 2010; Ostriker & Mckee 1988). In such cases as well the inverse relation between outflowing mass and the circular velocity of the galaxy still holds with a different scaling. Thus due to supernova explosions small mass galaxies would lose more gas and experience a strong negative feedback to the star formation compare to higher mass galaxies.

Hence, it is important to build a complete model of high redshift galaxy formation taking account of all the observational evidences, particularly the SNe feedback driven star formation in high redshift galaxies and their metal transport to the IGM. Numerical simulations are the best way to study all these together and a tremendous effort is going on (for example, Scannapieco et al., 2005 & 2006; Dave, Oppenheimer & Sivanandam, 2008; Dave, Oppenheimer, & Finlator, 2011; Scannapieco et al., 2012). However, present state of art hydrodynamic simulations are far from reality. They are constrained by the resolutions as well as the amount of physical processes that they can take account together (Scannapieco et al., 2012; Stringer et al. 2012). Here, we build an analytical model of star formation in the high redshift galaxies regulated by the feedback from SNe driven winds and try to explain the amount stellar mass and metals detected inside galaxies and the high redshift UV luminosity functions of Lyman-Break Galaxies (LBGs). In past, several authors have proposed semi-analytical models in order to understand the high redshift as well as low redshift galaxy formation process (White & Frenk, 1991; Kauffmann, White & Guiderdoni, 1993; Cole et al., 1994; Baugh et al, 1998; Somerville & Primack, 1999; Chiu & Ostriker, 2000; Granato et al 2000; Choudhury & Srianand, 2002; Baugh et al., 2005; Shankar et al 2006). These works clearly demonstrated the power of such semi-analytical modeling by predicting various observations

regarding high redshift universe. However, they have not derived a universal closed analytical form for the time evolution of star formation rate (SFR) in a single galaxy. Chiu & Ostriker (2000), Choudhury & Srianand (2002) and some of our earlier works (Samui et al., 2007, 2008; Jose et al., 2011) have used such a closed form without considering the SNe feedback and also not deriving their star formation model from first principle. Others have just considered star formation rate to be proportional to the available cold gas and not derived a single evolution equation for the evolution of the star formation rate including feedback. Here, we solve for the star formation rate in a closed form starting from very basic physics governing the star formation and taking account of the negative feedback from galactic outflows on the star formation in a self-consistent manner. This closed form will be very useful while fitting the photometric observations of high redshift galaxies in order to find their star formation history, stellar mass etc. Moreover, the new data are extended to much lower in stellar mass/luminosity and higher redshift where the process of reionisation is still going on. In one hand these low mass systems are the dominating sources of reionization. On the other hand they are much likely to prone to SNe feedback. Hence, it is timely to revisit feedback induced star formation in high redshift galaxies in the light of new improved data sets. Further, semi-analytical models are always useful as they are computationally inexpensive and help to understand the average universe very well. Also it is important to explore vast range of parameters that regulates the physical processes happening inside a galaxy.

The paper is organised as follows. In section 2 we clearly state our feedback induced star formation model in galaxies and how well it explains the stellar mass detected in dwarf galaxies to high mass galaxies. The mass-metallicity-SFR relation of galaxies is discussed in section 3. We present our model of UV luminosity function in section 4. We show our model predictions of UV luminosity functions of LBGs and compare that with observations in section 5. Finally we draw our conclusions with some discussions in section 6. Through out this paper we assume a Λ cold dark matter (Λ CDM) cosmology with the cosmological parameter as obtained by recent WMAP observation¹, i.e. $\Omega_\Lambda = 0.73$, $\Omega_m = 0.27$, $\Omega_b = 0.045$ and Hubble parameter $H_0 = 70$ km/s/Mpc.

2. Feedback induced Star formation in individual galaxy

We model the star formation rate including the feedback from SNe driven outflows in a galaxy as follows. We assume that the instantaneous star formation rate at a given time is proportional to the amount of cold gas present in the galaxy. Once the dark matter halo virialises it accretes baryonic matter and a fraction, f_* , of that becomes cold and available for star formation. The f_* can be thought of as star formation efficiency and is a free parameter in our model. The baryon accretion rate in a galaxy of total mass M at time t after the formation of dark matter halo is taken as

$$\frac{dM_g}{dt} = \left(\frac{M_b}{\tau} \right) e^{[-t/\tau]} \quad (1)$$

where M_g is the gas mass and $M_b = (\Omega_b/\Omega_m)M$ is the total baryonic mass in the halo. Further, τ is the dynamical time of the galaxy (Barkana & Loeb, 2001). We assume that the total gas mass in the galaxy is equal to the dark matter mass times the universal dark matter to baryon mass ratio. Note that integrating Eq. 1 from $t = 0$ to ∞ results $M_g = M_b$. The exponential form of the baryon accretion rate can be understood as follows. Once the dark matter halo virialises, the baryons are captured in the potential well and heated to virial temperature of the dark matter potential. In order to form stars the gas needs

¹For a list of Cosmological Parameters based on the latest observations see <http://lambda.gsfc.nasa.gov/product/map/current/parameters.cfm>

to cool and fall into the centre of the galaxy. If one assumes the rate of hot gas becoming cold is proportional to the amount of hot gas present, the increase in cold gas mass would follow an exponential form with time scale governed by the cooling time (t_{cool}). However, as already mentioned, this cold gas has to collapse into the centre of the galaxy in order to form stars. The collapse of the gas into the centre of dark matter halo is governed by the dynamical time scale of the gravitational potential. For most of the galaxy masses that we are interested, $t_{\text{cool}} \lesssim \tau$ (Silk, 1993). This is true even at the mean overdensity of the collapsed halo which is ~ 180 times the background density. Hence the effective cold gas accretion rate can be taken as an exponential form with time scale of the order of dynamical time scale for the system. Further note that the accretions of cold gas in galaxies has been found to be important observationally and also considered in previous semi-analytical models (i.e. Kauffmann et al. 1993, Shankar et al. 2006). Our exponential cold gas accretion rate tries to model that. Such an exponential form for the cold gas accretion rate has been also used by other semi-analytical works (for example see appendix of Shankar et al. 2006).

At a given time some gas would already be locked inside stars. Further, the massive stars are short lived and would explode as supernova after few times 10^7 yrs. These supernovae can drive the cold gas out of galaxy as galactic wind. We assume that the amount of gas mass driven out by the supernova in the form of wind is proportional to the instantaneous star formation rate, neglecting the time delay of $\lesssim 10^7$ yrs between the star formation and subsequent explosion of supernova, i.e.

$$\dot{M}_w = \eta_w \dot{M}_*. \quad (2)$$

Here, M_w is the wind mass; M_* is the star mass and over dot represents the time derivative. The proportionality constant η_w depends on the driving mechanism of outflows. For example, if the outflows are driven by the hot gas produced by the SNe, then $\eta_w \propto v_c^{-2}$, v_c being the circular velocity of the galaxy. Such outflows are referred to as energy driven outflows. If the hot gas loses its energy by radiative cooling, then outflows can be potentially driven by the pressure of cosmic rays produced in the SNe shocks. It was shown analytically in Samui et al. (2010) that in such cases $\eta_w \propto v_c^{-2}$ as well. However, if the momentum of the cooled gas helps in driving the outflow, $\eta_w \propto v_c^{-1}$. These are called momentum driven outflows. Detailed models of such supernova driven outflows can be found in Weaver et al. (1977), Ostriker & McKee (1988), Scannapieco et al. (2002), Veilleux, Cecil, & Bland-Hawthorn (2005), Samui et al. (2008).

Finally, taking account of the mass in stars, mass in outflows and baryonic mass accreted we can write down the star formation rate at time t after the formation of dark matter halo as

$$\frac{dM_*}{dt} = f_t \left[\frac{f_* M_g - M_* - M_w}{\tau} \right], \quad (3)$$

with f_t is some proportionality constant that governs the duration of star formation. Taking the time derivative of Eq. 3 and putting values of \dot{M}_g and \dot{M}_w from Eq. 1 and 2 respectively, we get

$$\begin{aligned} \frac{d^2 M_*}{dt^2} &= \frac{f_t}{\tau} \left[f_* \frac{dM_g}{dt} - \frac{dM_*}{dt} - \frac{dM_w}{dt} \right] \\ &= \frac{f_t}{\tau} \left[f_* \frac{M_b}{\tau} e^{-\frac{t}{\tau}} - \frac{dM_*}{dt} - \eta_w \frac{dM_*}{dt} \right]. \end{aligned} \quad (4)$$

Integrating this with the boundary condition that $dM_*/dt = 0$ and $M_* = 0$ at $t = 0$ we have

$$\frac{dM_*}{dt} = \frac{M_b f_* f_t}{\tau [f_t (1 + \eta_w) - 1]} \left[e^{-\frac{t}{\tau}} - e^{-f_t (1 + \eta_w) \frac{t}{\tau}} \right]. \quad (5)$$

Eq. 5 gives the analytical form of star formation rate in a galaxy at age t in presence of supernova feedback and is the backbone of our feedback induced star formation model. Note that putting η_w equals to zero would lead to star formation rate in a without feedback scenario and that form of star formation rate has been widely used in semi-analytical galaxy formation model in past by various authors (see Chiu & Ostriker, 2000; Choudhury & Srianand, 2002; Samui et al., 2007; Jose et al., 2011; Jose et al., 2013).

It is interesting to note that the total baryonic mass that will be eventually converted to stars is

$$M_*(t \rightarrow \infty) = \left(\frac{1}{1 + \eta_w} \right) M_b f_* \quad (6)$$

which is independent of f_t and inversely proportional to $1 + \eta_w$.

We have already mentioned that

$$\eta_w = \left(\frac{v_c}{v_c^0} \right)^{-\alpha}, \quad (7)$$

where v_c^0 is the circular velocity of the halo for which $\eta_w = 1$ and $\alpha = 2$ or 1 depending on whether outflows are energy driven/cosmic rays driven or momentum driven. Hence, for a small mass galaxy that has a lower circular velocity, η_w is large compare to a high mass galaxy with higher v_c . Thus from Eq. 6 it is clear that our model predicts a higher stellar mass fraction (M_*/M_b or equivalently M_*/M) in high mass galaxies and lower stellar mass fraction for small mass dwarf galaxies. The SNe feedback regulates the total amount of star formed in a galaxy. For small mass dwarf galaxies the SNe feedback is strong leading to a large decrease in the star formation in those galaxies. Large mass galaxies due to their large gravitational potential are less prone to the SNe feedback and suppression of star formation due to such feedback is small. Indeed, observationally we found such a correlation between the stellar mass and circular velocity/mass of galaxy.

In Fig. 1 we show our model predictions of stellar masses as a function of both circular velocity and mass of a galaxy along with the observational data. The observed data points are taken from McGaugh (2005), Stark et al. (2009), Walker et al. (2009) and Gerhard et al. (2001). Note that in absence of any feedback, one expects $M_* = f_*(\Omega_b/\Omega_m)M$ which would be a straight line as shown by the dotted lines in Fig. 1. From observational data itself it is obvious that small mass galaxies have very small amount of stars. At $M = 10^8 M_\odot$ the suppression is almost two orders of magnitude compared to the universal dark matter to baryon ratio whereas at $M = 10^{12} M_\odot$ the suppression is almost zero. Thus star formation models that do not take account of feedback fail to reproduce the observation. One must consider the negative feedback of SNe on subsequent star formation in a consistent way like in our model. We show our model predictions for $\alpha = 2$ (left panel) i.e. energy driven SNe feedback and $\alpha = 1$ i.e. momentum driven SNe feedback. The solid and dashed lines in both the panels are for $v_c^0 = 125$ km/s and 75 km/s respectively. We choose such normalisation as they provide a reasonable good fit to the data and also in Samui et al. (2010) such a normalisation naturally arises for Cosmic ray driven outflows (See Table 1 of Samui et al., 2010). We have assumed $f_* = 0.4$ for all the models. Note that with this choice of f_* , less than 20% of baryon mass is converted to star for $M \lesssim 10^{11} M_\odot$.

It is clear from the figure that our model predictions match quite well with the observed data. For high mass galaxies with $v_c \gtrsim 30$ km/s the errors in the measurements as well as the scatter in the data are small and we obtain a good fit to the observed data for both $\alpha = 2$ and 1. The spread in the data is within the statistical uncertainty of the model parameters. It is interesting to note that the observed data sample consists of different types of galaxies. While the Stark et al. (2009) galaxy samples are gas dominated spiral galaxies, the

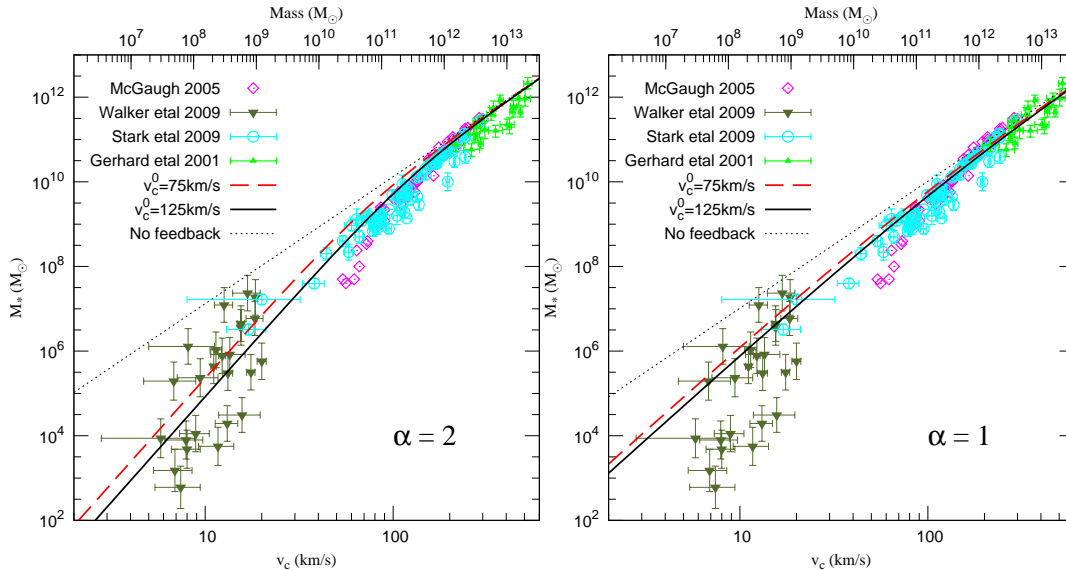


Figure 1: Stellar mass as a function of circular velocity and mass of the galaxy. The observed data points are taken from McGaugh (2005) (magenta diamonds), Stark et al. (2009) (cyan circles), Walker et al. (2009) (dark green reverse triangles) and Gerhard et al. (2001) (green triangles). The solid and dashed lines show our model prediction for $v_c^0 = 125$ km/s and 75 km/s respectively with $f_* = 0.4$. The left panel is for $\alpha = 2$ and right panel for $\alpha = 1$. The dotted line in both panels represents the no feedback scenario.

McGaugh et al. data consists of both gas dominated as well as gas poor star mass dominated galaxies. On the other hand, the Gerhard et al. (2001) samples are compendium of the early type galaxies. Hence our model reproduces the observed stellar mass fraction for different galaxy population with masses $M \gtrsim 10^{10} M_\odot$. For small mass dwarf galaxies with $v_c \lesssim 30$ km/s the observational points are quite scatter although our model predictions agree reasonably well especially for $\alpha = 2$. For $\alpha = 1$ it seems that additional feedbacks other than the SNe feedback are needed to suppress star formation even more in those galaxies in order to explain majority of the data points. However in any model the spread in the observational data is much more than the statistical uncertainty of the model parameters. Interestingly these dwarf galaxies are mostly satellite galaxies and they are likely to be affected by tidal stripping and radiative feedback from reionization that we discuss later while considering the luminosity function of LBGs. Hence, it is not surprising that our simple model of star formation including only the SNe feedback fails to explain the spread in the observed data for dwarf galaxies. Also note that for higher values of η_w one may expect the radiative cooling of the outflowing material to be important and the hot thermal gas that drives the outflows cools efficiently making the outflow a momentum driven one (see Samui et al. 2009 for details example of such outflows). However, our models show that $\alpha = 2$ is more favourable even for low mass dwarf galaxies which points to the fact that the outflows from dwarf galaxies are most likely not momentum driven outflows. Therefore, one must consider some alternative driving force for the outflows in these galaxies. In Samui et al. (2010) we showed that cosmic rays can provide such alternative with correct scaling of $\alpha = 2$.

In order to investigate this more we also consider the ratio of stellar mass to halo mass (SHM) as a function of halo mass. In Fig. 2 we show our model predictions along with observationally derived SHM ratio by Leauthaud et al. (2012) (green shaded region) and Moster et al. (2010) (cyan hatched area) with measurement uncertainty. Leauthaud et al. used deep COSMOS data along with halo occupation distribution model to constrain SHM ratio. Moster et al. derived the SHM ratio from N-body simulation with recent SDSS clustering data and galaxy galaxy lensing data. Even though there are slight mismatch in their derived SHM ratio, our model predictions match well considering the

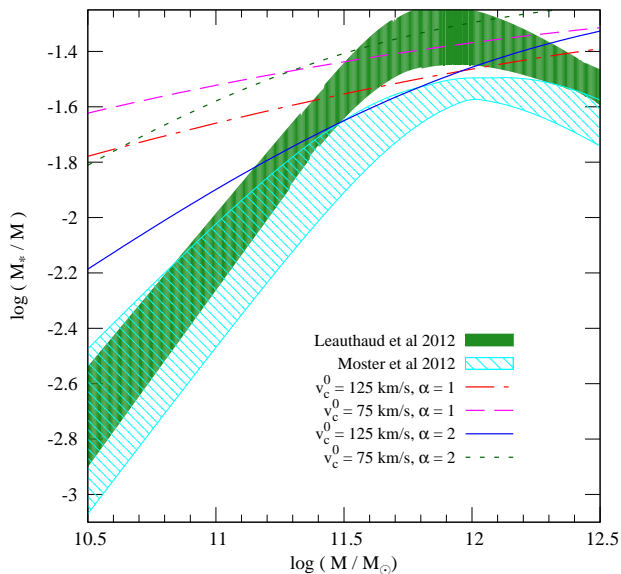


Figure 2: The stellar to halo mass ratio. The green shaded and cyan hatched areas are observationally derived SHM relation taken from Leauthaud et al. (2012) and Moster et al. (2010) respectively. Different lines are predictions from our various models. The blue solid and green dotted lines are for $\alpha = 2$ with $v_c^0 = 125$ and 75 km/s respectively. The dotted dashed red line and dashed magenta line are for $\alpha = 1$ with $v_c^0 = 125$ and 75 km/s respectively.

uncertainty in measurement. Here also we see that momentum driven cases ($\alpha = 1$) provide a poorer fit to the derived SHM ratio compared to $\alpha = 2$ models in low mass region. We wish to point out that the decrease in SHM ratio for $M \gtrsim 10^{12} M_\odot$ is due to AGN feedback that we have not considered here. Also the observed galaxies have a limiting stellar mass of $\log(M_*/M_\odot) = 8.7$ corresponds to $\log(M/M_\odot) \sim 11$ that has been used to derived the SHM. Hence one should not compare our model predictions with this particular observation beyond this mass limit.

3. Mass-Metallicity relation

In this section we focus on the gas phase metallicity of the high redshift galaxies in order to understand the observed mass-metallicity relation. The metallicity of a galaxy in our model can be calculated as follows. We assume that the amount of metals ejected by the supernova per unit of star formation is p and these metals are mixed with the ISM instantaneously. Suppose at a given time the metallicity of the ISM is Z . If at that instance δM_* amount of stars are formed then total gas mass reduced from the ISM is $\delta M_g = (1 + \eta_w)\delta M_*$. The second term arises due to the loss of gas through outflows. Note that we neglect the recycled gas that is returned by the supernova into the ISM as it is very small. For example, in a Salpeter IMF from $0.1 - 100 M_\odot$ the return fraction is less than 15%. Given δM_* of star formation, the amount of metal lost from the ISM is $Z(1 + \eta_w)\delta M_*$. However, supernova will produce $p\delta M_*$ metals. Hence total change of metal mass (M_h) in the ISM is

$$\delta M_h = [p - Z(1 + \eta_w)]\delta M_*.$$

Recall that $Z = M_h/M_g$. Differentiating this and using above relations we obtain

$$\begin{aligned} \delta Z &= \frac{\delta M_h}{M_g} - \frac{M_h}{M_g^2} \delta M_g \\ &= \left[\frac{p}{M_b - (1 + \eta_w)M_*} \right] \delta M_* \end{aligned} \quad (8)$$

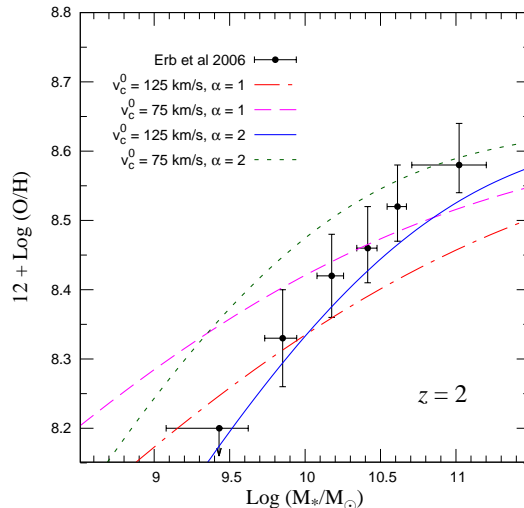


Figure 3: The gas phase metallicity as a function of stellar mass. The blue solid and green dotted lines are for $\alpha = 2$ with $v_c^0 = 125$ and 75 km/s respectively. The dotted dashed red line and dashed magenta line are for $\alpha = 1$ with $v_c^0 = 125$ and 75 km/s respectively. The Observed data points are taken from Erb et al., (2006).

Integrating this with boundary condition that the initial metallicity of the collapsed gas is Z_0 , we obtain

$$Z = Z_0 - \left(\frac{p}{1 + \eta_w} \right) \ln \left[1 - (1 + \eta_w) \frac{M_*}{M_b} \right] \quad (9)$$

In Fig. 3 we show our model prediction for stellar mass metallicity relation. Note that the stellar mass is obtained from Eq. 6 and metallicity is obtained from Eq. 9. The observed data points are taken from Erb et al. (2006) for the sample of galaxies at $z \sim 2$. We take $p = (0.6/50) M_\odot$ which means one supernova will form per $50 M_\odot$ of star formation and it will produce $0.6 M_\odot$ of Oxygen (Starburst99: Leitherer et al., 1999). Further, we assume $Z_0 = 0$. It is clear from the figure that our models reproduce the observed correlation very well. Especially, for the case of $\alpha = 2$ models, the two normalisation circular velocities namely $v_c^0 = 75$ and 125 km/s nicely bracket the observed correlation function. Predicted mass metallicity correlation by $\alpha = 1$ models is flatter than the observed values. Therefore, this correlation also favours the $\alpha = 2$ models compared to $\alpha = 1$ models which produce poorer fit to the observation. And we conclude that the wind feedback is the main driver to determine the amount of metals in galaxies.

As we have discussed early, recent observations have pointed out that the correlation of stellar mass and gas phase metallicity actually comes from a projection of more fundamental 3-D relationship between stellar mass, metallicity and star formation rate of galaxies. The offset seen in the mass metallicity relation between local universe and high redshift universe is due to selection bias of observing only higher star forming galaxies at high redshift (Mannucci et al. 2010). Hence any model of galaxy formation should be able to reproduce this fundamental 3-D relation. Indeed our models do predict such a correlation between stellar mass, metallicity and SFR. In Fig. 4 we show both projections of this relationship as predicted by our models along with the observational data taken from Mannucci et al. (2010). The top panels show metallicity as a function of stellar mass (the color shaded area) as obtained from all the four models discussed above (the parameters of each model is indicated in each panel). The color bar represent the star formation rate of the galaxy. In each panel the color coded curves are the observational data with same color indicator for the star formation rate. In the bottom panels we show the metallicity as a function of star formation rate for a range of stellar masses. It is obvious from the figure

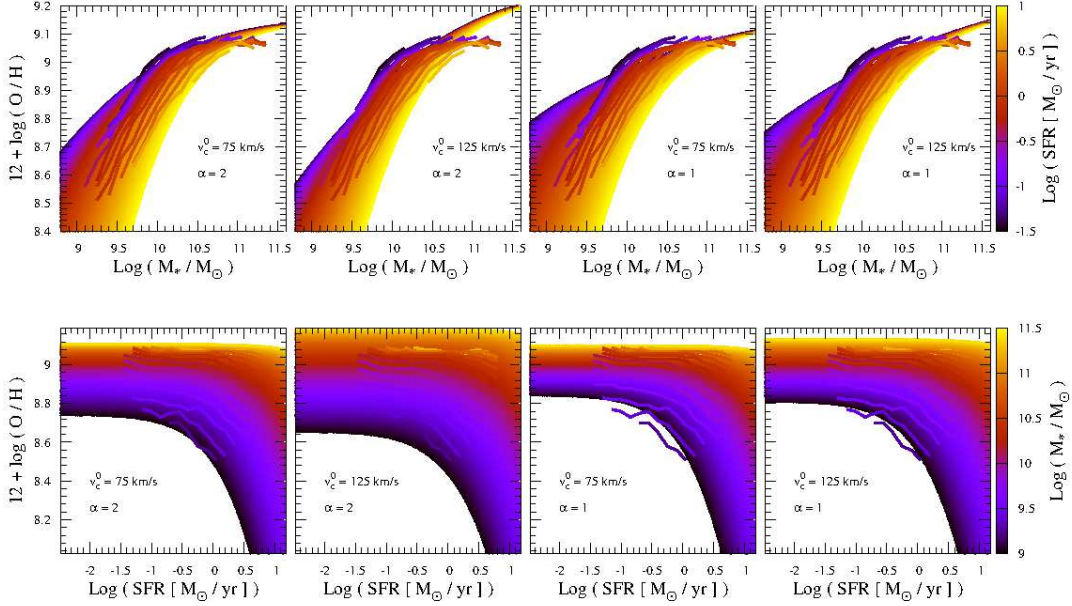


Figure 4: Projection of fundamental mass-metallicity-SFR relation. We show our model predictions for the mass metallicity SFR relation by the colour shaded area. The top panels show the metallicity as a function of stellar mass. The color indicates the star formation rate. In bottom panels we show the metallicity as a function of star formation rate. In these panels the color indicates the stellar mass. In all panels the observed fundamental mass metallicity SFR relation is shown by the same color coded solid curves taken from Mannucci et al. (2010).

that our models produce the 3-D correlation observed in galaxies. All our models produce the trend, i.e. for a given stellar mass, higher star forming galaxies have lower metallicity compared to low star forming counterparts or for a given star formation higher metallicity is obtained for higher stellar mass. However, it is interesting to point out that the model with $\alpha = 2$ and $v_c^0 = 75$ km/s provides the best fit with the observation. Note that in this case the model has to reproduce both the projections simultaneously. Like, the model with $\alpha = 2$ and $v_c^0 = 125$ km/s provide good fit with mass-metallicity relation but does not reproduce spread in SFR-metallicity relation. Both the models with $\alpha = 1$ unable to explain the correctly the observational data. We therefore conclude like in previous section that the observations are well reproduced by $\alpha = 2$ models again indicating the importance of cosmic ray driven winds.

4. Luminosity functions at high redshifts

After successfully explaining the stellar and metal mass detected in galaxies, we turn to the high redshift UV luminosity functions of LBGs. We broadly follow Samui et al. (2007 & 2009) to calculate high redshift luminosity functions. Below we briefly describe our model.

We obtain luminosity evolution of a galaxy undergoing a burst of one unit of star formation at a specific wavelength (say $\lambda = 1500$ Å) from population synthesis code “Starburst99” (Leitherer et al., 1999) assuming some initial mass function² for the stars formed. We convolve that with star formation rate of individual galaxy in our model (i.e. Eq. 5) to obtain the luminosity as a function of galaxy age (See Eq. 6 of Samui et al., 2007 and also Fig. 1 there). Note that the difference with Samui et al. (2007) model is that here we explicitly use the SNe feedback to the star formation. Further, all the light produced inside a

²We take a Salpeter initial mass function in the mass range $1 - 100 M_\odot$ throughout this paper.

galaxy by the stars do not reach to us due to presence of dust. A fraction, $1/\eta$, of total luminosity of the galaxy can be observed from earth.

We assume each luminous galaxy is formed inside a virialised dark matter halo provided the gas can cool and host star formation. The formation rate of dark matter halos per unit volume, $N(M, z)$, at a given redshift is calculated by taking the redshift derivative of Sheth-Tormen mass function (Sheth & Tormen, 1999). The Sheth-Tormen (ST) mass function provides a good fit to the numerical simulation data (Brandbyge et al., 2010) and hence we use it to calculate the formation rate of dark matter halos. Note that the time derivative of mass function provides total change in the number of halos; not just formation rate. One can extend Sasaki formalism (Sasaki, 1994) for Press-Schechter Mass function in order to get formation rate of halos from ST mass function. However, it is well known that naive extension of this formalism does not work for other mass functions (Samui et al., 2009; Mitra et al., 2011). Hence we use the simple time derivative to get the formation rate of halos with the assumption that it closely follows the formation rate. However, to show the effect of mass function on the predicted luminosity functions, we also consider Press-Schechter (PS) mass function with Sasaki formalism to calculate the formation rate of dark matter halos. In particular, we want to see if the conclusion of Samui et al. (2009) is still valid with the new feedback induced star formation model. The cumulative luminosity function, $\Phi(> L, z)$ for luminosity L at a given redshift z can be obtained from

$$\Phi(> L, z) = \int_z^\infty dz_c N(M, z_c) \Theta[L - L(M, z, z_c)]. \quad (10)$$

Here, $N(M, z_c)$ is the number of dark matter halos per unit volume between mass M and $M + dM$ and collapsed between redshift z_c and $z_c + dz_c$. The Heaviside theta function $\Theta[L - L(M, z, z_c)]$ ensures that the integral is contributed only by galaxies that are formed at redshift z_c and having luminosity, $L(M, z, z_c)$, greater than L (after correcting for dust reddening) at observe redshift z , with $z < z_c$. Taking derivative of Eq. 10 with respect to L and multiplying by the jacobi dM_{AB}/dL (M_{AB} is the magnitude in AB system (Oke & Gunn, 1983)) we get the luminosity functions, $\Phi(M_{AB}, z)$, at a given redshift.

In our model we calculate the reionization history and radiative feedback to the star formation in a self consistent way (for detail see Samui et al., 2007). A galaxy forming in the neutral region can cool with the help of atomic cooling if its virial temperature of the dark matter halo is greater than 10^4 K. Below this temperature a galaxy can cool and host star formation only in presence of molecular hydrogen. In this paper we consider only the atomic cooled halos as they are the main contributor to the luminosity functions in the observable range. In the ionised region of universe, due to the increase of Jeans mass, a galaxy can host star formation only if its virial velocity is greater than 35 km/s. We assume a complete suppression of star formation for $v_c \leq 35$ km/s and no suppression above $v_c = 95$ km/s. For intermediate mass range we adopt a linear fit from 1 to 0 (Broom & Loeb, 2002; Benson et al., 2002, Dijkstra et al., 2004). We also assume a suppression of star formation in high mass halos by a factor of $[1 + (M/10^{12} M_\odot)^3]^{-1}$ due to possible feedback from AGN (Bower et al., 2006; Best et al., 2006).

5. Constraining model parameters from observations

In this section we show our model predictions for the UV luminosity functions of LBGs and compare them with observations in the redshift range $1.5 \leq z \leq 8$. Note that two free parameters of our model, the star formation efficiency, f_* and dust reddening correction factor, η come as a product like f_*/η while calculating the luminosity of a galaxy and hence the luminosity function at a given redshift (we have assumed $f_t = 1$). We use χ -square minimization

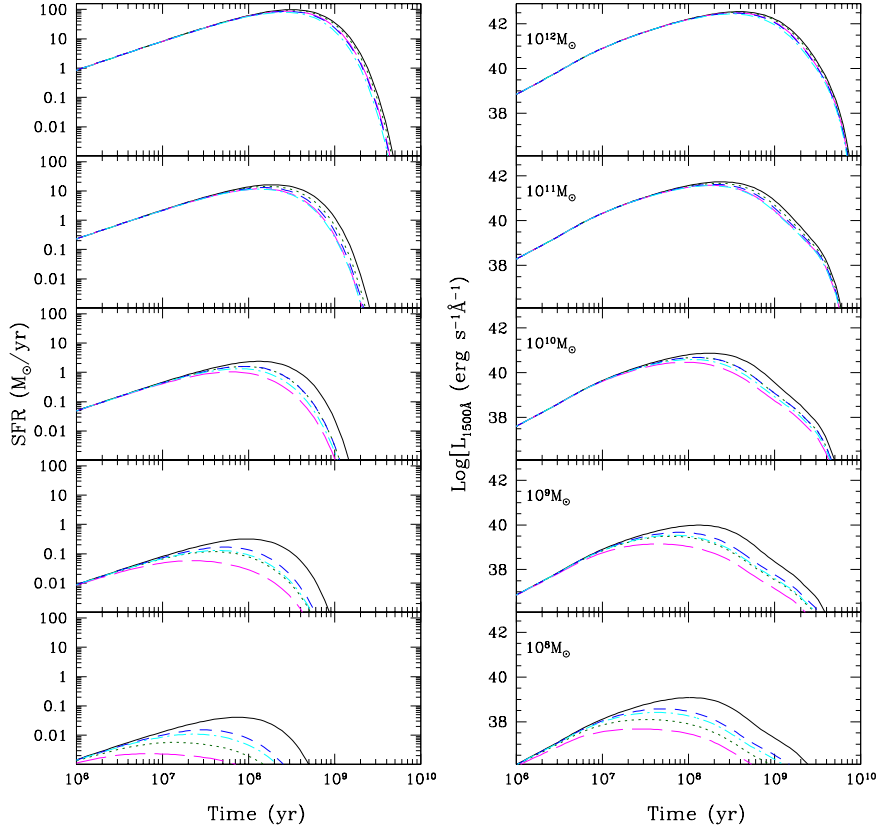


Figure 5: The evolution of star formation rate (left panels) and luminosity at 1500 \AA (right panels) of individual galaxies of masses 10^{12} , 10^{11} , 10^{10} , 10^9 and $10^8 M_{\odot}$ from top to bottom. The dark green dotted lines and magenta long dashed lines are for $\alpha = 2$ with $v_c^0 = 75$ and 125 km/s respectively. The blue short dashed curves and cyan dotted dashed curves are for $\alpha = 1$ with $v_c^0 = 75$ and 125 km/s respectively. In each panel we show, for comparison, the without feedback model (i.e. $\eta_w = 0$) with solid black lines.

technique to fit observed luminosity functions at different redshifts taking f_*/η as a free parameter. Taking this product (f_*/η) as independent of mass of the galaxy may seem simplistic. However, note that both f_* and η can depend on the mass of the galaxy (Bouwens et al., 2012). Since we can not disentangle one from other while calculating the luminosity we do not consider mass dependent f_* and/or η here. Further, η measures the amount of reddening due to dust. Observationally it has been found that the high redshift galaxies exhibit smaller amount of dust compared to their low redshift counterpart by measuring the UV continuum slope (Hopkins & Beacom, 2006; Bouwens et al., 2012). From physical point of view, high redshift galaxies should have less amount of metals and hence little dust. Thus, we expect that f_*/η should have different values at different redshift even if the efficiency remains same and we try to constrain this by fitting the observed UV luminosity function.

Before showing the luminosity functions at a given redshift, we show the star formation rate as obtained from Eq. 5 and resulting luminosity evolution of a single galaxy as a function of galaxy age. In Fig. 5, we show star formation rate (SFR) (left panels) and UV luminosity at 1500 \AA (right panels) for galaxies with masses 10^{12} , 10^{11} , 10^{10} , 10^9 and $10^8 M_{\odot}$ from top to bottom assuming collapsed redshifts of $z_c = 4, 6, 8, 10$ and 12 respectively. Note that z_c fixes the dynamical time scale τ (Barkana & Loeb, 2001) and we choose z_c such that the halo can collapse from a 3σ density fluctuation at z_c . We also take $f_t = 1$ for the rest of the paper. Note that changing f_t would change the duration of star

formation. Larger f_t means a shorter duration of star formation representing a burst mode of star formation and smaller f_t corresponds to a prolonged star formation scenario in the galaxy. In Fig. 5 we show models with $\alpha = 2$ & $v_c^0 = 125$ km/s (dark green dotted curves), $\alpha = 2$ & $v_c^0 = 75$ km/s (magenta long dashed curves), $\alpha = 1$ & $v_c^0 = 125$ km/s (blue short dashed curves), and $\alpha = 1$ & $v_c^0 = 75$ km/s (cyan dotted dashed curves). For comparison we also show the without feedback model ($\eta_w = 0$) with black solid line.

Fig. 5 nicely demonstrates that our SNe feedback models affect the star formation most in the low mass galaxies as η_w is higher in those galaxies. The maximum suppression of star formation happens for models with $\alpha = 2$ and $v_c^0 = 125$ km/s and the effect is minimum for models with $\alpha = 1$ and $v_c^0 = 75$ km/s. For $10^8 M_\odot$ galaxy the suppression is almost two orders of magnitude in star formation rate that results two orders of magnitude decrease in the maximum luminosity compare to no feedback model (bottom panels of Fig. 5). Note that peak of the star formation hence the luminosity also happens early in time with $t_{\text{peak}} = (\tau/\eta_w) \ln(1 + \eta_w)$. The suppression in star formation decreases with increasing galaxy mass; we see one order of magnitude suppression in peak star formation rate and also in maximum luminosity for galaxy of $M = 10^{10} M_\odot$ (middle panels of Fig. 5). For even higher mass galaxies SNe feedback has very little effect on the star formation and hence on the luminosity of the galaxy. One hardly notices the difference (less than factor 2) in star formation rate/luminosity for various feedback models with no feedback model for $10^{12} M_\odot$ galaxy (top panels of Fig. 5). Interestingly such kind of feedback effect due to the SNe on the star formation history of individual galaxies are also seen in full hydrodynamic simulations (Scannapieco et al., 2006)

Hence our SNe feedback model affects and regulates the star formation/luminosity of galaxies differentially, low mass galaxies get affected most and high mass galaxies least. Such a feedback would change the slope of the luminosity functions at different redshifts making them flatter. Indeed we see such flattening in the observational data of UV luminosity functions of LBGs. In Figs. 6 and 7, we show our model predictions of luminosity functions in the redshift range $1.5 \leq z \leq 8$ along with the observational data for ST and PS mass function respectively. The observed data points are taken from Oesch et al. (2010) ($z = 1.5, 1.9$ and 2.5), Reddy & Steidel (2009) ($z = 3$), Bouwens et al. (2007) ($z = 4, 5$ and 6) and Mannucci et al. (2007), Bouwens et al. (2008) and Bouwens et al. (2011) for $z = 7$ and 8 . Note that the open triangles at $z = 4, 5$ and 6 suffer from incompleteness problem (see Bouwens et al., 2007) and hence we do not consider them while fitting. The fitted values of f_*/η along with the best fit χ -square per degree of freedom (dof) are tabulated in Table 1. Note that all our models predict the reionization histories that are well within the available observational constraints. In particular, for all our models, we obtain redshift of reionization greater than 6 as inferred from the observations of Lyman-alpha forest in distant quasars (Fan et al., 2006) and electron scattering optical depth within one sigma of WMAP 7yrs results ($\tau_e = 0.087 \pm 0.014$) (Komatsu et al., 2011). It is important to note that the feedback induced star formation model reduces the star formation severely in low mass galaxies. These galaxies are the main sources of the UV photon that causes the reionization of the IGM and lower the star formation lesser the UV photon production. However, the fraction of UV photon that can escape from a galaxy and cause the ionisation of the IGM is poorly constrained especially for low mass galaxies. We observe that using a escape fraction of 0.2 leads to a similar reionization history (and electron scattering optical depth to the reionization) for the feedback induced star formation models compared to the no feedback model with escape fraction of 0.1. This value of escape fraction of UV photon is in good agreement with recent numerical results (Wise & Cen 2009; Pawlik et al. 2009; Yajima et al. 2009) as well as observations (Bouwens et al. 2010). Thus, our feedback models also produce the reionization history with reasonable physical parameters.

We first consider the ST mass function. It is clear from the Fig. 6 and also

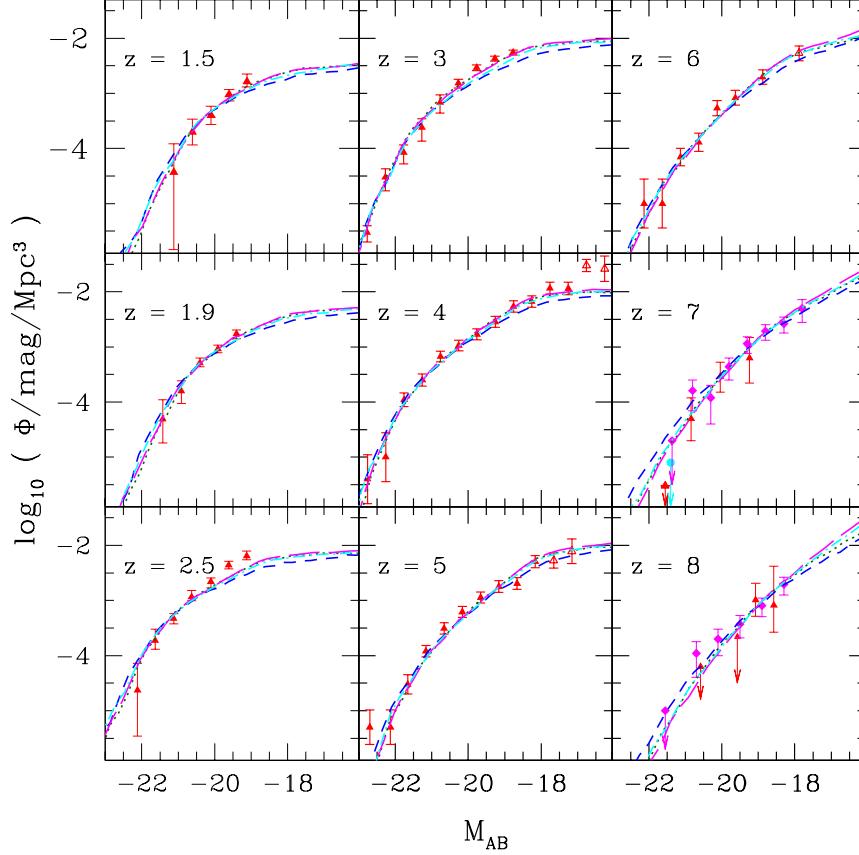


Figure 6: The observed luminosity functions for $1.5 \leq z \leq 8$ along with our model predictions for Sheth-Tormen mass function. The best fit values of f_*/η are tabulated in Table 1. We show our model predictions for $\alpha = 2$ with $v_c^0 = 75$ km/s (dark green dotted curves) and $v_c^0 = 125$ km/s (blue short dashed curves) and $\alpha = 1$ with $v_c^0 = 75$ km/s (magenta long dashed curves) and $v_c^0 = 125$ km/s (cyan dotted dashed curves). The observed data points are taken from Oesch et al. (2010) (red triangles at $z = 1.5, 1.9$ and 2.5), Reddy & Steidel (2009) (red triangles at $z = 3$), Bouwens et al. (2007) (red triangles at $z = 4, 5$ and 6), Bouwens et al. (2008) (red triangles at $z = 7$), Mannucci et al. (2007) (cyan bullet at $z = 7$) and Bouwens et al. (2011) (magenta diamonds at $z = 7$ and 8).

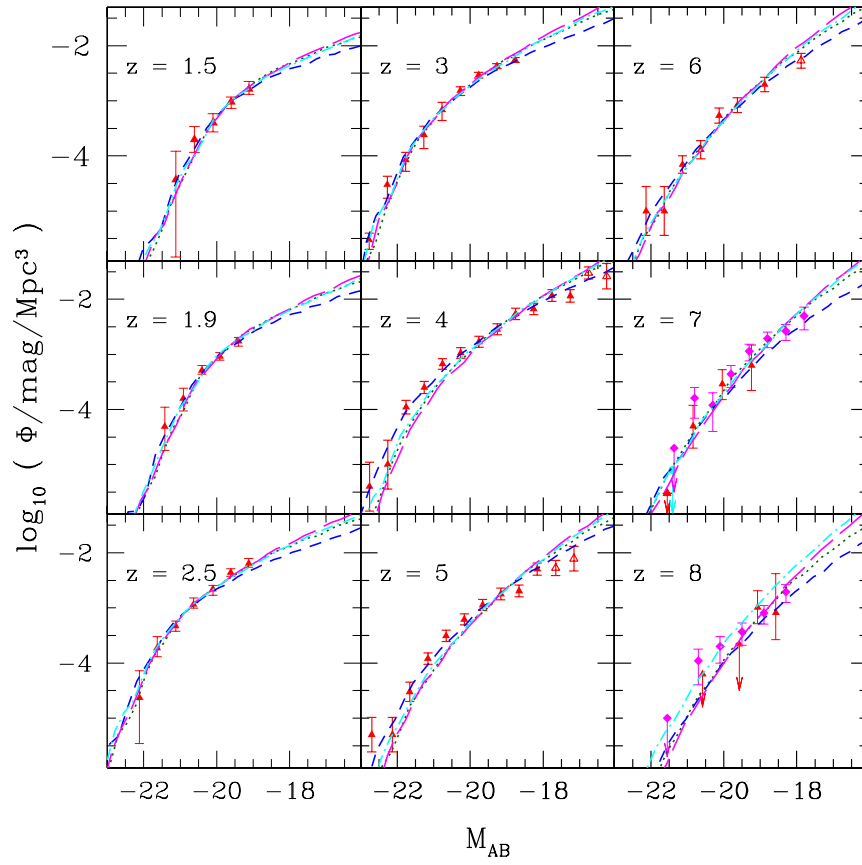


Figure 7: Same as Fig. 6 but for Press-Schechter mass function with Sasaki formalism.

z	$\alpha = 2, v_c = 125 \text{ km/s}$		$\alpha = 2, v_c = 75 \text{ km/s}$		$\alpha = 1, v_c = 125 \text{ km/s}$		$\alpha = 1, v_c = 75 \text{ km/s}$	
	f_*/η	χ^2/dof	f_*/η	χ^2/dof	f_*/η	χ^2/dof	f_*/η	χ^2/dof
ST derivative								
1.5	0.048 ± 0.003	0.81	0.037 ± 0.002	0.28	0.053 ± 0.003	0.56	0.044 ± 0.003	0.40
1.9	0.049 ± 0.002	0.89	0.038 ± 0.001	0.24	0.054 ± 0.002	0.49	0.045 ± 0.001	0.22
2.5	0.079 ± 0.003	4.12	0.064 ± 0.002	2.44	0.087 ± 0.003	3.05	0.074 ± 0.002	2.46
3	0.059 ± 0.001	6.40	0.056 ± 0.001	1.51	0.067 ± 0.001	4.13	0.062 ± 0.001	1.80
4	0.062 ± 0.002	1.11	0.052 ± 0.001	0.40	0.068 ± 0.002	0.46	0.060 ± 0.001	0.38
5	0.050 ± 0.001	0.98	0.041 ± 0.001	1.36	0.052 ± 0.001	1.14	0.045 ± 0.001	1.51
6	0.062 ± 0.002	0.68	0.052 ± 0.002	0.55	0.066 ± 0.002	0.56	0.057 ± 0.002	0.51
7	0.120 ± 0.006	0.38	0.083 ± 0.004	0.38	0.086 ± 0.004	0.40	0.072 ± 0.003	0.50
8	0.114 ± 0.007	0.26	0.080 ± 0.004	0.45	0.099 ± 0.005	0.55	0.083 ± 0.004	0.65
PS Sasaki								
1.5	0.029 ± 0.001	0.12	0.023 ± 0.001	0.25	0.031 ± 0.001	0.21	0.026 ± 0.001	0.24
1.9	0.034 ± 0.001	0.26	0.027 ± 0.001	0.64	0.037 ± 0.001	0.68	0.031 ± 0.001	0.62
2.5	0.067 ± 0.002	1.45	0.054 ± 0.001	0.37	0.074 ± 0.002	0.50	0.063 ± 0.002	0.28
3	0.061 ± 0.001	1.24	0.050 ± 0.001	1.55	0.065 ± 0.001	0.78	0.057 ± 0.001	1.57
4	0.074 ± 0.001	1.02	0.051 ± 0.001	4.55	0.066 ± 0.001	4.58	0.052 ± 0.001	6.76
5	0.076 ± 0.001	2.20	0.052 ± 0.001	5.95	0.069 ± 0.001	5.18	0.058 ± 0.001	6.44
6	0.115 ± 0.004	0.63	0.090 ± 0.003	0.71	0.110 ± 0.003	0.77	0.096 ± 0.002	0.80
7	0.179 ± 0.008	0.32	0.113 ± 0.004	0.69	0.134 ± 0.006	1.02	0.110 ± 0.004	1.21
8	0.248 ± 0.014	0.32	0.153 ± 0.007	0.80	0.185 ± 0.009	0.86	0.150 ± 0.007	1.06

Table 1: The best fit values of f_*/η for all our models along with the best fit χ -square per degree of freedom for $1.5 \leq z \leq 8$. We quote $1 - \sigma$ error in the measurements of f_*/η .

from Table 1 that our models reasonably explain the UV luminosity functions of LBGs in a vast redshift range of $1.5 \leq z \leq 8$. The flattening observed in the low end of luminosity functions ($M_{AB} \gtrsim 18$) particularly in the redshift range of $4 \leq z \leq 6$ are well explained by the SNe feedback and the radiative feedback that we assume. Except for $z = 2.5$ and 3 the best fit χ -square per degree of freedom is very close to unity or less than unity. This demonstrates how well our model predictions match with observations. In general, for all our models, values of f_*/η show an increasing trend with redshift with some exceptions at $z = 2.5$ and $z = 5$ that we discuss later. This is in accord with the concordance model of structure formation. If one assumes a fixed $f_* = 0.4$ which provides a reasonable fit to the observational data for the stellar mass in galaxies (See Fig. 1) one sees that the value of $1/\eta$ increases with increasing redshift. This means in the past the amount of dust present in a galaxy was less on average. As the universe became older the amount of metals in galaxies increased making them more dusty and hence more difficult to detect. Also the mean values of η obtained assuming $f_* = 0.4$ is in good agreement with the observation of Reddy et al. (2012). They found a mean value of $\eta = 5.2$ at $z \sim 2$.

Further we notice that the models with $v_c^0 = 75$ km/s provide a better fit to the observational data compare to the models with $v_c^0 = 125$ km/s for both $\alpha = 2$ and 1 in all redshifts except for $z = 5$ and 8 . In particular, for $z \leq 4$ the models with $v_c^0 = 75$ km/s fit the faint end slope of the luminosity functions better than models with $v_c^0 = 125$ km/s. For $z \geq 5$ both the models over fit the observational data as best fit values of χ^2 per degree of freedom are less than unity and hence it can not identify the best fit model. At $z = 2.5$ none of our models provide a good fit to the observational data. The bright end of the luminosity function is well explained by our models. However, they fail to reproduce the last two data points at the low luminosity end. Interestingly we found the faint end slope of the observed luminosity function at $z = 2.5$ is quite steep compared to $z = 3$ luminosity function. It is very unlikely to change the slope within such a short time. We expect future improve observations would clarify this dispute. This also leads to a higher value of f_*/η at $z = 2.5$ compared to values that are obtained for $z \geq 3$.

The observed luminosity function at $z = 3$ clearly favours the models with $v_c^0 = 75$ km/s for both $\alpha = 2$ and 1 . The models with $v_c^0 = 125$ km/s fail to reproduce the faint end slope of the observed luminosity function. Such a signature is also seen in case of $z = 1.5$ and $z = 1.9$. The feedback in those models (i.e. models with $v_c^0 = 125$ km/s) are very strong to suppress the star formation in low mass galaxies and hence fail to produce enough number of low luminosity galaxy to explain the observed luminosity functions at $z \leq 3$.

At $z = 4$ we see that our models provide a reasonable fit to the observed data. The model with $\alpha = 2$ and $v_c^0 = 125$ km/s does not fit the last four observational points in the low luminosity end and hence has maximum value for the best fit χ^2 . However, none of our models able to fit the last two data points in the low luminosity end (the open triangles). As already mentioned above these two data points suffer major uncertainty in measurements and we do not consider them while fitting. If future observations confirm these data points then we have to change our model in order to explain the low luminosity end of the luminosity function at $z = 4$.

All our models well explain the observed luminosity function at $z = 5$. However, we see from Table 1 that the best fit values of χ^2 per dof at this redshift are quite higher than unity except for model with $\alpha = 2$ and $v_c^0 = 125$ km/s for which best fit $\chi^2/\text{dof} = 0.98$. We observe that the data point at $M_{AB} = -18.66$ has unusually low value of $\Phi(M_{AB})$ compare to its neighbouring data points and contribute significantly to the best fit χ^2 values. It also leads to a lower value of f_*/η compared to $z = 4$. Ignoring this data point all our models fit the observed luminosity function with best fit χ^2 per dof values close to unity.

For redshift $z \geq 6$ our model predictions match very well with the observed data. Note that the errors in the measurements are very high especially at $z = 7$

and 8. Thus all models provide good fit to the data with best fit χ^2 per degree of freedom much less than unity. We expect that future observations would reduce the error bars and extend the measurements to even lower luminosity allowing us to put further constraints on star formation models. In passing we note that we can not distinguish two feedback models namely energy driven/cosmic ray driven SNe winds (i.e. $\alpha = 2$) and momentum driven SNe winds ($\alpha = 1$) with the present observational data of UV luminosity functions of LBGs at various redshifts. The reason behind this is that the two models differ maximum in low mass dwarf galaxies where the η_w can be different by more than factor 10. It was shown in Samui et al. (2007) that the present observable range of luminosity functions are contributed mostly by the galaxies with mass $M \gtrsim 10^{10} M_\odot$. At this mass the η_w for models with energy driven SNe wind is larger only by factor 3 (2) in case of $v_c^0 = 125$ km/s ($v_c^0 = 75$ km/s) compared to models with momentum driven wind and hence can not be distinguished by the present observational data due to the large errors in the measurements.

We now turn to the luminosity function as obtained using PS halo mass function and compare with ST mass function. Fig. 7 shows the predicted luminosity functions and the fitted parameters are tabulated in Table 1. It is obvious from the figure that PS mass function also produces the shape and evolution of luminosity function correctly. However, Table. 1 shows that in most of the redshift we considered (i.e. except $z = 2.5$ & 3), PS mass function provide a poorer fit compared to ST mass function. Thus the flattening of luminosity functions at low luminosity end can only be explain due to SNe feedback and can not be explain with different form of the halo mass function. Further, our previous conclusions regarding the halo mass function remain same i.e. ST mass function provides a better understanding of high redshift luminosity functions compared to PS mass function.

6. Discussions and Conclusions

We have built improved semi-analytical models of high redshift galaxy formation where star formation is regulated by the feedback due to SNe driven outflows. We consider two models of feedback; one in which the outflows are driven by the thermal energy of the SNe remnants and in second the hot gas loses its thermal energy due to radiation and the momentum of the gas helps in driving the outflow. The effect of SNe feedback to the star formation is calculated in a self-regulated manner. We derive an analytical form for the star formation rate in a galaxy that is regulated by the SNe feedback. Given the star formation rate in individual galaxy we calculate high redshift galaxy luminosity functions.

Our feedback induced star formation models are successful in explaining the observed stellar mass in galaxies of different types with mass range $10^{10} M_\odot \lesssim M \lesssim 10^{13} M_\odot$. For low mass dwarf galaxies our simple model of star formation including SNe feedback produces the trend in correlation between the observed stellar mass and circular velocity but fails to explain the spread in it. Other feedback mechanisms are expected to operate on such small mass galaxies in order to understand the observations. Our models also produces the observed ratio of stellar mass to halo mass as a function of halo masses as obtained from recent SDSS data. Further, our models emphasize the importance of alternative driver of galactic outflows such as cosmic rays. The amount of metals detected in high redshift galaxies is well estimated by our models which demonstrates that the metal mass in a galaxy is vastly determined by the outflows. The 3-D correlation between gas phase metallicity, stellar mass and star formation rate is well explained by our feedback dominated star formation model showing the importance of SNe feedback in building this observed relationship in galaxies.

The observed UV luminosity functions of LBGs at $1.5 \leq z \leq 8$ are well explained with our feedback models. Especially the flattening observed at low end of the luminosity functions arises naturally with our feedback model. In

absence of such feedback one would produce more low mass galaxies and fail to reproduce the observed data points. The models with $v_c^0 = 75$ km/s provide a better fit to the observational data compared to $v_c^0 = 125$ km/s especially at low redshift (the characteristic circular velocity, v_c^0 , fixes the normalisation of our feedback model). This implies that the supernova feedback affects the star formation in galaxies more compare to ionisation feedback for high mass galaxies. For galaxies with $v_c \gtrsim 90$ km/s one expects to have no effect of ionization feedback to the star formation where as SNe feedback reduces the star formation by 40% in the same galaxies (taking $v_c^0 = 75$ km/s). The present observational data of high redshift luminosity functions is not good enough to distinguish a thermal energy driven outflow from a momentum driven outflow. We need to reduce the error in the measurements and extend the data to even lower luminosity end where these two models behave differently. Moreover, the flattening of the luminosity functions can not be explained as the difference between the form of halo mass function that one uses to calculate the formation rate of halos (like PS or ST mass function). It can only be understood due to SNe feedback.

Hence, our feedback regulated star formation model can explain a vast range of observations of high redshift universe. Having such kind of simple analytical form for physically motivated star formation of individual galaxy is very helpful for determining the star formation rate of high redshift galaxies by fitting spectral energy distribution (SED) with several broad band photometry. In such case the star formation history is very important to determine several physical quantities such as the star formation rate, stellar mass, age of the galaxy etc. In general one considers a constant star formation model or an exponentially decaying one in such fits. However, Reddy et al. (2012) showed that high redshift galaxies ($1.5 \leq z \leq 2.6$) are more expected to have a rising star formation history and very young age when they are detected. Our successful star formation models actually predict such kind of rising star formation history at the young age and then gradually decreasing star formation history after a fraction of dynamical time. We expect that using our model in such SED fitting would lead to a better fit to the observational data and also provide more clearer picture of high redshift galaxies.

Since SNe feedback is one of the main improvement of our model over past, it is important to investigate its effect on the global metal pollution. Especially by the fact that in low mass galaxies that dominate in the metal production at high redshift should have a cosmic ray pressure driven outflows, one should see how far this model can explain the global metal budget. We hope to address that in future.

acknowledgements

The author thanks Kandaswamy Subramanian and Raghunathan Srikanand for very useful discussions. The author also thanks anonymous referee for his/her useful comments that helped a lot to improve the quality of the paper.

References

- [1] Barkana, R., Loeb, A. 2001, PhR, 349, 125
- [2] Baugh, C. M., Cole, S., Frenk, C. S., Lacey, C. G., 1998, ApJ, 498, 504
- [3] Baugh C. M., Lacey C. G., Frenk C. S., Granato G. L., Silva L., Bressan A., Benson A. J., Cole S., 2005, MNRAS, 356, 1191
- [4] Benson, A. J., Lacey, C. G., Baugh, C M., Cole, S., Frenk, C. S., 2002, MNRAS, 333, 156

- [5] Best, P. N., Kaiser, C. R., Heckman, T. M., Kauffmann, G., 2006, MNRAS, 368, L67
- [6] Bouwens, R. J., Illingworth, G. D., Franx, M., Ford, H., 2007, ApJ, 670, 928
- [7] Bouwens, R. J., Illingworth, G. D., Franx, M., Ford, H., 2008, ApJ, 686, 230
- [8] Bouwens, R. J., et al., 2010, ApJ, 708L, 69
- [9] Bouwens, R. J. et al., 2011, ApJ, 737, 90
- [10] Bouwens, R. J. et al, 2012, ApJ, 754, 83
- [11] Bower, R. G., Benson, A. J., Malbon, R., Helly, J. C., Frenk, C. S., Baugh, C. M., Cole, S., Lacey, C. G., 2006, MNRAS, 370, 645
- [12] Brandbyge, J., Hannestad, S., Haugbille, T., Wong, Y. Y. Y., 2010, JCAP, 09, 014
- [13] Bromm, V., Loeb A., 2002, ApJ, 575, 111
- [14] Chiu W. A., Ostriker J. P., 2000, ApJ, 534, 507
- [15] Choudhury, T. R., Srianand, R., 2002, MNRAS, 336, L27
- [16] Cole, S., Aragon-Salamanca, A., Frenk, C. S., Navarro, J. F., Zepf, S. E., 1994, MNRAS, 271, 781
- [17] Cox, Donald P., 1972, ApJ, 178, 159
- [18] Cullen, F., Cirasuolo, M., McLure, R. J., Dunlop, J. S., 2013, arXiv1310.0816
- [19] Dave, R., Oppenheimer, B. D., Finlator, K., 2011, MNRAS, 415, 11
- [20] Dave, R., Oppenheimer, B. D., Sivanandam, S., 2008, MNRAS, 391, 110
- [21] Dijkstra, M., Haiman, Z., Rees, M., Weinberg, D. H., 2004, ApJ, 601, 666
- [22] Erb, D. K., Shapley, A. E., Pettini, M., Steidel, C. C., Reddy, N. A., Adelberger, K. L., 2006, ApJ, 644, 813
- [23] Fan, X., Strauss, M. A., Richards, G. T. et al., 2006, AJ, 131, 1203
- [24] Granato, G. L., Lacey, C. G., Silva, L., Bressan, A., Baugh, C. M., Cole, S., Frenk, C. S., 2000, ApJ, 542, 710
- [25] Garnett, D. R., 2002, ApJ, 581, 1019
- [26] Gerhard, O., Kronawitter, A., Saglia, R. P., Bender, R., 2001, AJ, 121, 1936
- [27] Gunn J. E., Peterson B. A., 1965, ApJ, 142, 1633
- [28] Hopkins, A. M., Beacom, J. F., 2006, ApJ, 651, 142
- [29] Jose, C., Samui, S., Subramanian, K., Srianand, R., 2011, PhRvD, 83, 3518
- [30] Jose, C., Subramanian, K., Srianand, R., Samui, S., 2013, MNRAS, 429, 2333
- [31] Kauffmann, G., White, S. D. M., Guiderdoni, B., 1993, MNRAS, 264, 201
- [32] Kewley, L. J., Ellison, S. L., 2008, ApJ, 681, 1183
- [33] Kobayashi, C., Springel, V., White, S. D. M., 2007, MNRAS, 376, 1465
- [34] Komatsu, E. et al., 2011, ApJS, 192, 18

- [35] Leauthaud A. et al., 2012, ApJ, 744, 159
- [36] Lee, H., Skillman, E. D., Cannon, J. M., Jackson, D. C., Gehrz, R. D., Polomski, E. F., Woodward, C. E., 2006, ApJ, 647, 970
- [37] Leitherer. C., et al., 1999, ApJS, 123, 3
- [38] Lequeux, J., Peimbert, M., Rayo, J. F., Serrano, A., Torres-Peimbert, S., 1979, A&A, 80, 155
- [39] Mannucci, F., Buttery, H., Maiolino, R., Marconi, A., Pozzetti, L., 2007, A&A, 461, 423
- [40] Mannucci, F., Cresci, G., Maiolino, R., Marconi, A., Gnerucci, A., 2010, MNRAS, 408, 2115
- [41] Mannucci, F., et al., 2009, MNRAS, 398, 1915
- [42] Martin, C. L., 1999, ApJ, 513, 156
- [43] Martin, C. L., 2005, ApJ, 621, 227
- [44] McGaugh, S. S., 2005, ApJ, 632, 859
- [45] Mitra, S., Kulkarni, G., Bagla, J. S., Yadav, J. K., 2011, BASI, 39, 563
- [46] Mortlock et al., 2011, Nature, 474, 616
- [47] Moster, B. P. et al., 2010, ApJ, 710, 903
- [48] Oesch, P. A et al., 2010, ApJ, 725, 150
- [49] Oke, J. B. and Gunn, J. E., 1983, ApJ, 266, 713
- [50] Ostriker, J. P., McKee, C. F., 1988, Rev. Modern Physics, 60, 1
- [51] Pettini, M., Shapley, A., Steidel, C.C., et al. 2001, ApJ, 554, 981
- [52] Pawlik, A. H., Schaye, J., van Scherpenzeel, E., 2009, MNRAS, 394, 1812
- [53] Reddy, N. A., Steidel, C. C., Fadda, D., Yan, L., Pettini, M., Shapley, A. E., Erb, D. K., Adelberger, K. L., 2006, ApJ, 644, 792
- [54] Reddy, N. A., Steidel, C. C., 2009, ApJ, 692, 778
- [55] Reddy, N. et al., 2012, ApJ, 744, 154
- [56] Samui, S., Srianand, R., Subramanian, K., 2007, MNRAS, 377, 285
- [57] Samui, S., Subramanian, K., Srianand, R., 2008, MNRAS, 385, 783
- [58] Samui, S., Subramanian, K., Srianand, R., 2009, NewA, 14, 591
- [59] Samui, S., Subramanian, K., Srianand, R., 2010, MNRAS, 402, 2778
- [60] Sasaki S., 1994, PASJ, 46, 427
- [61] Savaglio, S., et al., 2005, ApJ, 635, 260
- [62] Scannapieco, C. et al, 2012, MNRAS, tmp, 2970
- [63] Scannapieco, C., Tissera, P. B., White, S. D. M., Springel, V., 2005, MNRAS, 364, 552
- [64] Scannapieco, C., Tissera, P. B., White, S. D. M., Springel, V., 2006, MNRAS, 371, 1125
- [65] Scannapieco, C.; Tissera, P. B.; White, S. D. M.; Springel, V., 2008, MNRAS, 389, 1137

- [66] Scannapieco, E., Ferrara, A., Madau, P., 2002, ApJ, 574, 590
- [67] Shankar, F., Lapi, A., Salucci, P., De Zotti, G., Danese, L., 2006, ApJ, 643, 14
- [68] Sheth R. K., Tormen G., 1999, MNRAS, 308, 119
- [69] Silk, J., 1993, PNAS, 90, 4835
- [70] Somerville, R. S., Primack, J. R., 1999, MNRAS, 310, 1087
- [71] Stark, D. V., McGaugh, S. S., Swaters, R. A., 2009, AJ, 138, 392
- [72] Steidel, C. C., Adelberger, K. L., Shapley, A. E., Pettini, M., Dickinson, M.; Giavalisco, M., 2003, ApJ, 592, 728
- [73] Stringer, M. J., Bower, R. G., Cole, S., Frenk, C. S., Theuns, T., 2012, MNRAS, tmp, 2923
- [74] Tremonti, C. A. et al, 2004, ApJ, 613, 898
- [75] Veilleux, S., Cecil, G., Bland-Hawthorn, J., 2005, ARA&A, 43, 769
- [76] Walker, M. G., Mateo, M., Olszewski, E. W., Pearrubia, J., Wyn E. N., Gilmore, G., 2009, ApJ, 704, 1274
- [77] Weaver, R., McCray, R., Castor, J., Shapiro, P., Moore, R., 1977, ApJ, 218, 377
- [78] White S. D., Frenk C. S., 1991, ApJ, 379, 52
- [79] Wise, J. H., Cen, R. 2009, ApJ, 693, 984
- [80] Wyithe, J. S. B., Loeb, A., Carilli, C., 2005, ApJ, 628, 575
- [81] Yajima, H., Umemura, M., Mori, M., Nakamoto, T., 2009, MNRAS, 398, 715